Broadband Ultra-high Frequency Sensor for Multi-condition Partial Discharge Detection in High-voltage Equipment

Zulbirri Faizol[1], Farid Zubir[1†], Salah I. Yahya[2], Mohd H. Ahmad[3], Norhafezaidi M. Saman[3], Osman Ayop[4], Arshad Karimbu Vallappil[5], and Mohamad Z. Abd Aziz[6]

[1]Wireless Communication Centre, Faculty of Electrical Engineering, Universiti Teknologi Malaysia, Johor Bahru, Malaysia

[2]Department of Computer Technology Engineering, College of Technical Engineering, Al-Hadba University, Mosul, Iraq

[3]Institute of High Voltage and High Current, Faculty of Electrical Engineering, Universiti Teknologi Malaysia, Johor Bahru, Malaysia

[4]Advanced RF and Microwave Research Group, Faculty of Electrical Engineering, Universiti Teknologi Malaysia, Johor Bahru, Malaysia

[5]Department of Electrical Engineering, Faculty of Engineering, Islamic University of Madinah, Madinah, Saudi Arabia

[6]Faculty of Electronics and Computer Technology and Engineering, Universiti Teknikal Malaysia Melaka, Melaka, Malaysia

***Abstract*—Partial discharge (PD) is a localized electrical phenomenon occurring within degraded insulation of high-voltage (HV) equipment, where its discharge mechanisms and radiated electromagnetic characteristics vary significantly across air, oil, and gas-insulated systems. Undetected PD can gradually damage insulation and eventually lead to equipment failure and power outages. Therefore, researchers are urged to develop reliable detection methods that are effective across different insulation media to ensure the safe operation of power systems. In this study, ultra-high frequency electromagnetic signals generated from PD activity are analyzed using an external log-periodic dipole array (LPDA) antenna. This research focuses on broadband sensing and considers the PD activity in various insulation materials, including air, oil, and gas. Moreover, lumped inductors are added to achieve a more compact antenna design without compromising the performance. The proposed LPDA antenna is fabricated on an FR-4 substrate and evaluated using a vector network analyzer. As a result, a reflection coefficient below −10 dB from 0.4 GHz to 2 GHz with a directional gain of 4–6 dBi is obtained, which satisfies the IEC 62478 standard. The results demonstrated that the proposed miniaturized LPDA antenna is effective for PD detection in different insulation environments.**

ARO-The Scientific Journal of Koya University
Vol. XIV, No. 1 (2026), Article ID: ARO.12846. 13 pages
DOI: 10.14500/aro.12846
Received 20 January 2026; Accepted 26 April 2026
Regular research paper: Published: 10 May 2026
†Corresponding author's e-mail: faridzubir@utm.my

***Index Terms*—Broadband sensing, High-voltage system monitoring, Inductor loading, Log-periodic dipole array antenna, Partial discharge.**

I. Introduction

Electrical insulation can slowly degrade and eventually fail during normal operation without proper monitoring. Therefore, reliable electrical insulation plays an important role in terms of the safety and stability of high-voltage (HV) equipment and power systems. Condition monitoring systems are implemented to reduce the risks by enabling early fault detection and improving diagnostic accuracy (Stone, 2012; Riera-Guasp, Antonino-Daviu, and Capolino, 2014). In this context, partial discharge (PD) is a commonly used indicator of insulation degradation and forms the basis of many condition monitoring techniques for HV equipment. PD is a localized electrical breakdown that occurs within the insulation of HV assets. If undetected, it can speed up insulation aging and lead to catastrophic insulation failure (Wu, et al., 2015). Conventional PD measurements and testing have been carried out based on electrical detection techniques defined in the IEC 60270 standard (Tenbohlen, Gulski, and Koltunowicz, 2016). While effective in controlled laboratory environments, these methods face limitations during real-world applications due to electromagnetic interference and external noise. To improve PD detection under such conditions, non-conventional techniques have been developed using PD-related physical phenomena, such as chemical by-products, acoustic detection, optical detection, and ultra-high

frequency (UHF) electromagnetic radiation (Duval, 2002; Descoeudres, et al., 2004; Biswas, et al., 2012). However, each approach has certain limitations in practical use.

Chemical detection is restricted to laboratory testing and can be inaccurate since it utilizes indirect measurements of by-products instead of PD itself (Kusumoto, et al., 1980). Acoustic detection is non-intrusive but sensitive to environmental noise and has low sensitivity to weak PD signals (Ilkhechi and Samimi, 2021). Optical detection is immune to electromagnetic interference, but is limited by sensor availability and requires direct line-of-sight to the PD discharge (Schwarz, Muhr, and Pack, 2005). Among these methods, UHF detection stands out due to its strong resistance to electromagnetic interference, which makes it suitable for on-site applications (Hoshino, et al., 2006; Tenbohlen, et al., 2008). In certain insulation media, such as oil, PD pulses can have rise times of less than one nanosecond. This produces electromagnetic signals in the UHF range of 300 MHz to 3 GHz, as defined in the IEC 62478 standard (Standard, 2000).

The behavior of PD signals varies depending on the insulation medium. In air, PD usually appears as corona or surface discharges with lower energy and wider radiation spread. In oil, internal and sharp-edge discharges produce stronger PD signals with clear UHF frequency features. In gas-insulated switchgear (GIS), PD caused by particles or surface discharges generates fast electromagnetic signals with less signal loss. These differences affect signal transmission and detection in practical UHF PD measurements. UHF detection was first applied to GIS in 1988 and later extended to transformers and HV cables (Hampton and Meats, 1988; Rutgers and Fu, 1997; Ahmed and Srinivas, 2002).

Effective UHF PD detection requires sensors that are capable of capturing wideband electromagnetic signals across various insulation environments while maintaining good sensitivity and directional performance. These sensors are commonly implemented as antennas, including spiral, fractal, microstrip, and log-periodic dipole array (LPDA) antennas (Mishra, et al., 2015; Wang, Wang and Li, 2016; Ashari and Khayam, 2017; Wang, et al., 2017; Wang, et al., 2020; Yadam, Sarathi and Arunachalam, 2022; Hu, et al., 2023; Muru and Setijadi, 2023; Uwiringiyimana, Khayam and Montanari, 2024).

As an example, a coplanar waveguide-fed UHF microstrip antenna for PD detection in GIS is reported in (Kong, et al., 2024). The design is realized on an FR-4 substrate ($\varepsilon r = 4.4$, thickness 1.6 mm), incorporating a trident-shaped feed and chamfered edges to enhance bandwidth. It achieved an operating range of 500–1120 MHz with a VSWR < 2, an average gain of 3.4 dB, and a peak gain of 4.6 dB, exhibiting nearly omnidirectional radiation. Experimental validation against corona and internal air-gap discharges confirmed effective PD detection with a high signal-to-noise ratio. In the work of (Ahmed, et al., 2024), a UHF planar antenna for PD detection in medium-voltage GIS using eco-friendly HFO(E)/CO_2 mixtures is proposed. The antenna is fabricated on an FR-4 substrate, achieving a wide operating band of 370–1300 MHz with a reflection coefficient below −10 dB, fully covering the UHF range relevant to PD emissions, and an average gain of 3.1 dBi, with omnidirectional radiation. The antenna is reported to have a higher signal-to-noise ratio and sensitivity compared to a high-frequency current transformer (HFCT) sensor.

Moreover, (Ardila-Rey, et al., 2024) reported a bioinspired UHF antenna for PD detection in HV equipment. This FR-4-based antenna is inspired by a dragonfly wing structure to provide wideband performance in a compact form. The antenna covered 0.35–2.1 GHz with a reflection coefficient, S_{11}, below −10 dB. Experimental tests on surface PD in epoxy resin and corona discharge in oil confirmed the reliable detection of weak PD signals and better sensitivity compared to Vivaldi and monopole antennas. (Salah, et al., 2022) introduced a compact double-layer printed Hilbert fractal UHF antenna for PD detection in oil-filled power transformers. The FR-4-based antenna operated in several UHF bands at 0.67–1.04 GHz, 1.4–2.0 GHz, 2.3–2.89 GHz, and 3.1–4.0 GHz, with an S_{11} below −10 dB. Experiments are conducted in an oil-filled tank with four artificial PD defects, including corona in air, sharp edge in oil, surface discharge, and internal void discharge. The results obtained demonstrated that different PD types generate different UHF signals, which allows defect differentiation with PD detection up to 40 cm.

In addition, (Chakravarthi, et al., 2021) presented a compact LPDA antenna for PD detection in transformers. The antenna consisted of seven dipole elements printed on both sides of an FR-4 substrate. A compact size is achieved using shaped dipole arms and optimized element placement, while added capacitance improves bandwidth and impedance matching. The antenna covers a frequency range of 0.5–2.2 GHz with a nearly constant gain of 4 dBi across 0.8–2.2 GHz. The experiment validated the effectiveness of the antenna to detect PD from different defect types, including particle movement, corona, free metallic particles, and surface discharges.

Recent work in PD detection has focused on compact UHF sensors, printed planar antennas, and improved noise immunity to support installation in transformers and GIS. Many recent designs reduce size using geometric modifications or printed structures, but often at the cost of bandwidth or radiation stability. However, existing research on UHF PD detection is limited to specific insulation media or discharge types, which restricts a complete analysis of PD behavior in air, oil, and gas-insulated systems. Some reported antennas also suffer from limited bandwidth and sensitivity. Considering the challenges, this work presents a miniaturized LPDA antenna for PD detection, tested and analyzed in various insulation environments. To achieve a compact antenna design, a lumped element approach is utilized, which is proven to be effective in size reduction and performance improvement (Luo, Pereira, and Salgado, 2011; Su, 2018; Xia, Li, and Xue, 2020; Chishti, et al., 2023). With this approach, the proposed LPDA antenna operates over a wide frequency range from 0.44 GHz to 2.75 GHz with an impedance bandwidth of 2.31 GHz, which lies within the UHF PD detection range in IEC 62478. The antenna indicates good impedance matching and reliable performance

by maintaining a VSWR below 2 and S_{11} below −10 dB. Unlike many reported antenna designs that focus on a single insulation environment or limited frequency range, the proposed antenna is experimentally validated across oil, air, and gas media. The combination of inductive miniaturization, wide frequency range, and multi-detection represents the main contribution of this work.

II. Design of The Proposed Antenna

The IEC 62478 standard defines the UHF range for PD detection as 300 MHz to 3 GHz. Covering this wide band ensures a reliable detection of different PD phenomena, especially in gas-insulated systems. In this work, a broadband antenna operating from 400 MHz to 2000 MHz is developed. While not covering the specified UHF band defined in the standard, the range is chosen as a practical trade-off between antenna size, complexity, and overall performance.

The antenna design process starts with a conventional LPDA structure designed to operate within the UHF PD detection band. After verifying the baseline impedance bandwidth and gain performance, size reduction was introduced through inductive reactive loading. Lumped inductors were inserted along the dipole arms to increase the electrical length of the antenna elements, allowing resonance to be maintained at lower frequencies without increasing physical dimensions. Parametric sweeps were conducted to optimize the inductor value and placement position. Following this, the dipole elements were modified into U-shaped structures to further reduce the overall footprint while preserving current distribution and radiation characteristics. Through iterative optimization of geometry and reactive loading, the final design achieved significant size reduction while maintaining broadband performance and stable gain.

The proposed LPDA antenna is fabricated on a double-sided FR-4 substrate (εr = 4.2, tan δ = 0.015) with a thickness of 1.6 mm. Both the radiating elements and ground plate are made using a 0.035 mm thick copper layer. The substrate material influences antenna performance through its dielectric constant and loss tangent, which affect impedance matching, bandwidth, and radiation efficiency. Higher permittivity enables size reduction but may increase dielectric losses, whereas low-loss materials improve efficiency and stability. Therefore, appropriate substrate selection is important for reliable practical operation.

The antenna consists of several dipole elements that decrease in size toward the front, which results in radiation mainly in the backward direction, known as backfire radiation. The largest dipole at the rear is designed to be half a wavelength at the lowest operating frequency, whereas the element dimensions, including length (l), width (w), and distance (d), are calculated using Equation (1) based on the scaling factor (τ) (Balanis, 2016).

$$\tau = \frac{l_n}{l_{n+1}} = \frac{w_n}{w_{n+1}} = \frac{d_n}{d_{n+1}} \quad (1)$$

Besides the scaling factor (τ), several design parameters also influence the shape and frequency behavior of the LPDA antenna, as defined in Equations (2) to (6) (Balanis, 2016). Based on the equations, the apex angle (α) is first determined to control the antenna's opening size, length, gain, and operating bandwidth. A bandwidth correction factor (B_{ar}) is then calculated to find the effective design bandwidth (B_s). Next, the required number of elements (N) is chosen, and the dipole lengths (l) are then optimized by considering the dielectric properties of the substrate. The final optimized dimensions, including the effect of inductors, are summarized in Table I.

$$B_{ar} = 1.1+7.7(1-\tau)^2 \cot \alpha \quad (2)$$

$$B_s = BB_{ar} = B[1.1 + 7.7(1-\tau)^2 \cot \alpha] \quad (3)$$

$$N = 1 + \frac{\ln B_s}{\ln \frac{1}{\tau}} \quad (4)$$

$$l = 0.5 \times \frac{v}{f} \quad (5)$$

$$v = \frac{c}{\sqrt{\varepsilon_r}} \quad (6)$$

To reduce the physical size of the proposed LPDA antenna, two techniques, including inductor loading and patch bending, are utilized. A single dipole antenna is first simulated to study the effect of inductive loading. The position and value of the inductors are adjusted separately to identify their effects on the resonant frequency of the antenna. Initially, a fixed value inductor is placed at different positions along the dipole, at 0.1, 0.3, 0.5, 0.7, and 0.9 of the dipole length. The inductance value is then varied from 3 nH to 51 nH after identifying the best position. After adding the inductors, the element dimensions and spacing are adjusted while maintaining the fundamental LPDA antenna structure and design principles.

A patch bending technique is then introduced to further reduce the length of the antenna. Each dipole element is

TABLE I
Parameters of the Proposed Log-Periodic Dipole Array Antenna with Inductors

Number of elements, *n*	Length of elements, *l* (mm)	Width of elements, *w* (mm)	Distance between elements, *d* (mm)	Inductor, *I* (nH)
1	19.24	2.68	6.70	2.2
2	22.64	3.15	7.88	3.0
3	26.64	3.71	9.27	3.0
4	31.34	4.36	10.91	3.0
5	36.87	5.13	12.83	3.0
6	43.38	6.04	15.09	3.0
7	51.03	7.11	17.75	3.0
8	60.04	8.36	20.88	4.1
9	70.63	9.83	24.57	5.6
10	83.09	11.56	28.90	5.6
11	97.75	13.60	34.00	3.0
12	115.00	16.00	40.00	4.1
13	135.29	18.82	47.06	9.9

http://dx.doi.org/10.14500/aro.12846

divided into three segments to form a U-shaped structure. In CST Microwave Studio, the antenna shape is modeled using a 3D polygon by defining the geometry through equations. The curve is traced using the curve-tracing tool and then converted into a copper patch element.

The effects of both methods on the size reduction and overall performance of the antenna are examined and reported in this work, and several key performance parameters, including S-parameters, radiation patterns, and gain, are evaluated. The final U-shaped LPDA antenna design with integrated inductors is shown in Fig. 1.

III. Results

This section presents the results and discussion for the proposed LPDA with integrated inductors. The effect of inductor position and value on antenna resonance is investigated. For each configuration, simulated S_{11}, radiation patterns, realized gain, and received power are analyzed. In addition, the operational bandwidth of each design is quantified and discussed.

The lumped inductors act as reactive loading elements that increase the effective electrical length of the dipole arms without increasing the physical size of the antenna. This loading shifts the resonance to lower frequencies, and the antenna size will be smaller. Parametric studies on inductor placement and values were conducted to observe impedance matching and bandwidth.

A. Effect of Inductor Position and Value on Antenna Resonance

The location of the inductor on the dipole arm directly affects how the antenna resonates. When the inductor is placed near the feed point, the dipole acts longer, which shifts the resonance to a lower frequency. On the other hand, if the inductor is placed closer to the end of the dipole, the effect is weaker, and the resonance becomes almost the same as the dipole without an inductor. Fig. 2 shows the comparison of S_{11} results based on the placement of the inductor.

Fig. 3 depicts the comparison of the S_{11} simulation results with various inductor values. Varying the inductor value changes the effective electrical length of the dipole. A higher inductance value increases the electrical length and shifts the resonant frequency to lower values. Smaller inductance values result in only a slight downward shift and generally maintain a wider bandwidth. In contrast, larger inductance values cause a more significant frequency shift but often lead to narrower bandwidth and degraded impedance matching due to higher quality factor and parasitic effects.

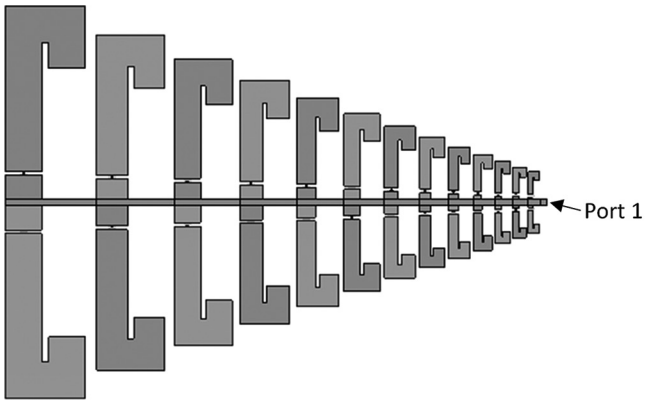

Fig. 1. The proposed design of the U-shaped log-periodic dipole array antenna with inductors.

B. Simulation and Measurement Results of Proposed LPDA Antenna

The antenna is fabricated on a 300 × 220 mm^2 FR-4 substrate, achieving a 63.3% size reduction as shown in Fig. 4a. In Fig. 4b, simulation results show an impedance bandwidth of 0.46–2.0 GHz (125.2%) with $S_{11} < -10$ dB, whereas measurements indicate an extended range of 0.44–2.75 GHz (144.8%). Multiple resonant dips confirm

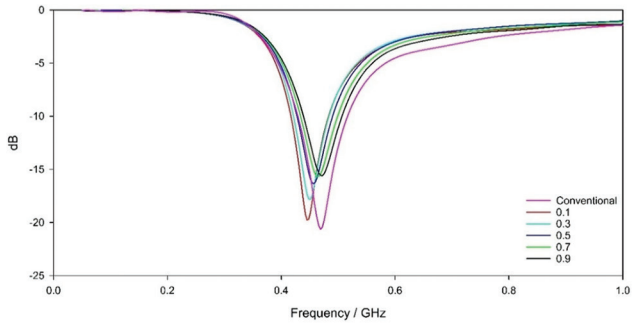

Fig. 2. Reflection coefficient of dipole antenna with inductor position at different fractions of the element length at 0.1, 0.3, 0.5, 0.7, and 0.9 of the dipole length.

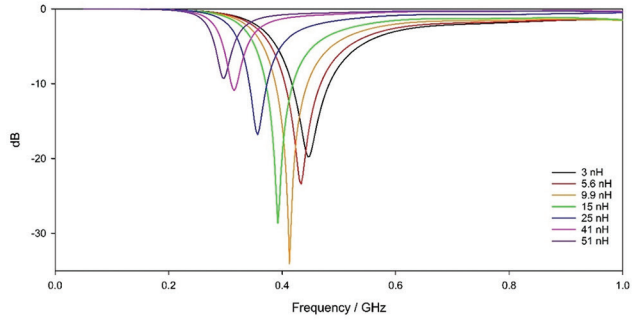

Fig. 3. S_{11} results of different inductor values for dipole antennas.

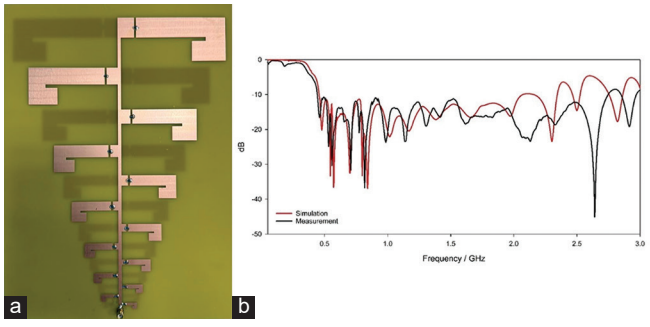

Fig. 4. (a) Fabrication of the U-Shaped patch log-periodic dipole array antenna and (b) simulated and measured S_{11}.

wideband impedance matching, with discrepancies between simulated and measured responses attributed to fabrication tolerances, inductor parasitics, and connector losses.

Fig. 5 presents the simulated and measured radiation patterns of the proposed U-shaped patch LPDA antenna at 0.5, 1.0, and 1.3 GHz. At 0.5 GHz, both results exhibit a wide beam with low directivity, although the measured pattern shows minor fluctuations. At 1.0 GHz, the beam becomes narrower and more directional, with measurements confirming stronger forward radiation but with less uniformity. At 1.3 GHz, the radiation is most focused, with simulations showing the narrowest main lobe and measurements following the same trend, albeit with additional sidelobes.

Fig. 6 shows the realized gain of the proposed LPDA antenna, which remains stable between 4 and 5 dBi across most of 0.4–2.0 GHz, with peaks above 5 dBi around 0.6–0.8 GHz and 1.1 GHz. The result demonstrates low gain at 400 MHz and 2 GHz due to the absence of a reflector at the largest element and the absence of a director at the smallest element, respectively.

IV. Experimental Setup And Results For PD Detection

The purpose of this study is to evaluate the proposed LPDA antenna for detecting electromagnetic signals produced by PD activity. Experiments are conducted under different conditions to validate its performance, as shown in subsection A to assess detection capability in oil, air, and gas environments, and subsection B to identify the types of PD generated in oil and air media.

A. PD Detection in Different Experimental Setups

The performance of the proposed LPDA antenna for PD detection is validated through experimental comparison with commercial antennas. For oil and air configurations, the acquired PD signals are compared with those obtained using the Watson W-881 whip antenna, which is widely employed in industry for PD monitoring. For gas conditions, the proposed antenna is evaluated against the PDU-G2 external antenna as shown in Fig. 7.

Fig. 8 shows the measured S_{11} comparison between the proposed LPDA antenna and two commercial antennas. The proposed antenna exhibits consistently better impedance matching across the operating frequency range, with S_{11} mostly maintained below −10 dB, indicating superior wideband performance. In contrast, the Watson W-881 antenna shows limited bandwidth with weaker matching at higher frequencies, whereas the PDU-G2 antenna demonstrates multiple resonant points but less stable impedance behavior across the band.

The comparison serves as a practical benchmark for assessing the effectiveness and reliability of the proposed antenna in detecting PD signals. Before performing the performance evaluation against a commercial whip antenna, PD activity is first measured using the conventional IEC 60270 method, which involves a coupling capacitor and measuring impedance. The measuring impedance is used to convert high-frequency PD pulses into measurable voltage signals and serves as a reference for verifying PD presence and characteristics before antenna testing.

IEC 60270 measurement is carried out using a 0–220V voltage regulator (variac) connected to an 80 kV HV transformer. The applied voltages are set to 35 kVrms in oil, 10 kVrms in air, and 17 kVrms in GIS, all operating at 50 Hz, and a 6.1 kΩ resistor connected in series on the secondary side to limit the current. Calibration is performed using a PD pulse calibrator before the unit under test (UUT) is energized to ensure accurate measurement. A 100 pF coupling capacitor and a 40 nF voltage divider capacitor are used as an overvoltage protection for the measuring equipment. The measuring impedance is connected to the PD detection equipment, whereas the coupling capacitor is linked to the UUT to initiate PD activity. The experiment setup is illustrated in Fig. 9.

For the oil and air experiments, a needle-to-plane electrode configuration is employed to generate corona and surface discharges, respectively. In the GIS, several metallic nails are placed inside the chamber to simulate free conducting particles, a common defect type noted in IEC standards. To evaluate antenna sensitivity, the proposed antenna is positioned at a distance of 100 cm from the PD

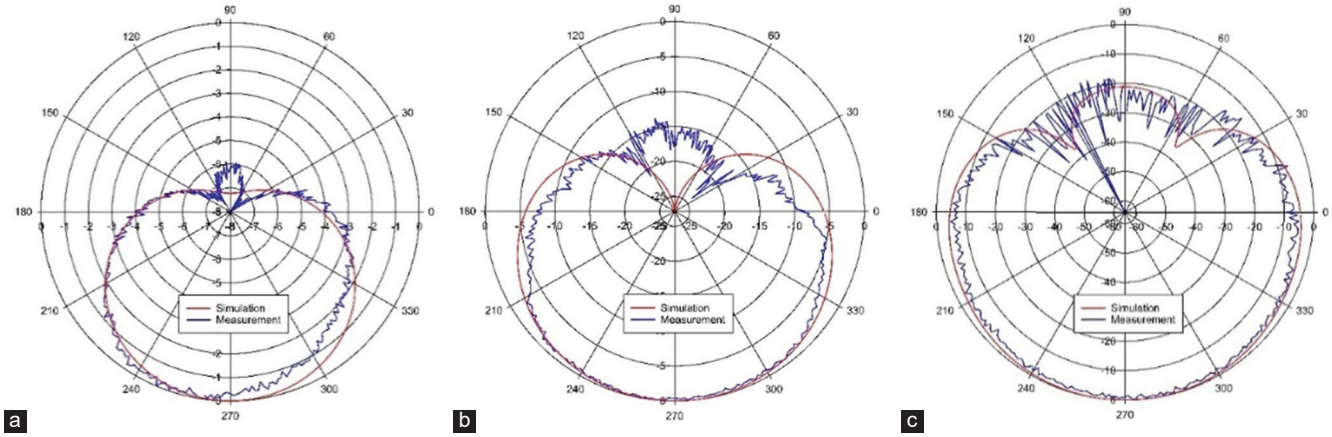

Fig. 5. Radiation pattern of proposed log-periodic dipole array antenna for (a) 0.5 GHz, (b) 1 GHz, and (c) 1.3 GHz.

http://dx.doi.org/10.14500/aro.12846

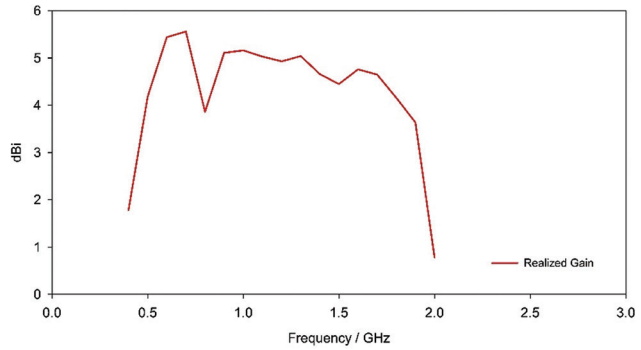

Fig. 6. Realized gain of the proposed log-periodic dipole array antenna.

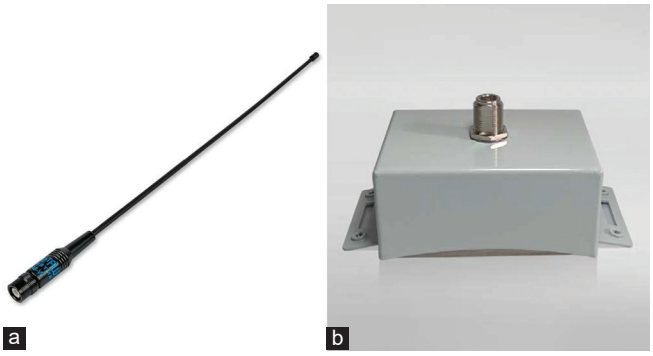

Fig. 7. Commercial antenna for detecting partial discharge in (a) oil and air conditions and (b) gas conditions.

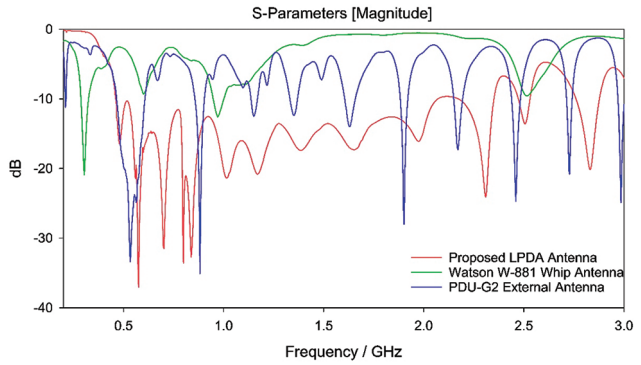

Fig. 8. Measured S_{11} performance comparison of the proposed log-periodic dipole array antenna against Watson W-881 and PDU-G2 commercial antennas.

source in the oil and air setups. For the GIS experiment, the antenna is fixed at a distance of 40 cm from the inspection window, whereas the commercial PDU-G2 antenna is mounted on the GIS flanges. Fig. 10 depicts the UUT used to generate PD.

Fig. 11a compares the background noise with PD signals detected at 100 cm using the Watson W-881 whip antenna, where multiple peaks rise above the noise floor with stronger activity in the lower and mid-frequency ranges. Fig. 11b presents the corresponding results for the proposed antenna, which also shows distinct PD peaks above the noise floor. Compared to the commercial whip, the proposed antenna provides clearer separation at higher frequencies, confirming its enhanced capability to distinguish PD activity from background noise.

Fig. 12 shows the zero-span analysis of PD detection at 536 MHz using both the commercial and proposed antennas at a distance of 100 cm in oil. The commercial antenna registers clear pulses with peak levels around −60 dBm, exceeding the noise floor of −80 dBm, whereas the proposed antenna records slightly stronger peaks at −57 dBm. Compared to the commercial sensor, the proposed antenna captures a higher number of PD signals, although with less steady pulse behavior.

Based on Fig. 13, both the commercial and proposed antennas successfully captured PD pulses. The commercial antenna shows clear peaks around −76 dBm above a baseline level of −91 dBm. In comparison, the proposed antenna produces stronger signals with peaks around −65 dBm and a similar baseline, which indicates better separation between signal and background noise.

Based on Fig. 14, the commercial antenna detects two PD pulses at approximately −85 dBm and −77 dBm, which are only slightly above the noise level. In comparison, the proposed antenna detects stronger signals, with a highest peak of about −65 dBm and another peak near −74 dBm, which indicates better sensitivity.

Fig. 15a and b present the frequency spectra obtained using the commercial whip antenna and the proposed LPDA antenna, respectively. Both antennas successfully captured PD activity above the noise floor; however, the proposed antenna exhibits stronger and more distinct peaks, particularly in the lower and mid-frequency ranges, indicating improved sensitivity. In contrast, the commercial antenna produces weaker responses with narrower separation from background noise.

At 434 MHz and a distance of 100 cm from the PD source, Fig. 16 shows that both antennas detected PD activity with clear peaks above the noise floor. The commercial antenna detects peaks around −69 dBm, whereas the proposed antenna shows slightly stronger peaks near −67 dBm. The higher signal level indicates that the proposed antenna is better at capturing surface discharge signals in air, which are usually stronger at lower frequencies.

As shown in Fig. 17, both antennas detect PD pulses at 499 MHz, but with different signal levels. The commercial antenna produces peaks around −78 dBm with a noise floor of −88 dBm, which results in limited separation and weaker signals. In comparison, the proposed antenna records stronger peaks near −76 dBm and more frequent pulses, which indicates better sensitivity and clearer PD detection.

At 510 MHz and a distance of 100 cm from the PD source, Fig. 18 shows the clear differences from the results of both antennas. The commercial antenna records pulses with moderate amplitudes, with peaks around −76 dBm. Although the pulses are spread over the time window, they remain clearly above the −90 dBm noise floor, confirming the detection of surface discharge activity. In contrast, the proposed U-shaped LPDA antenna produced stronger and

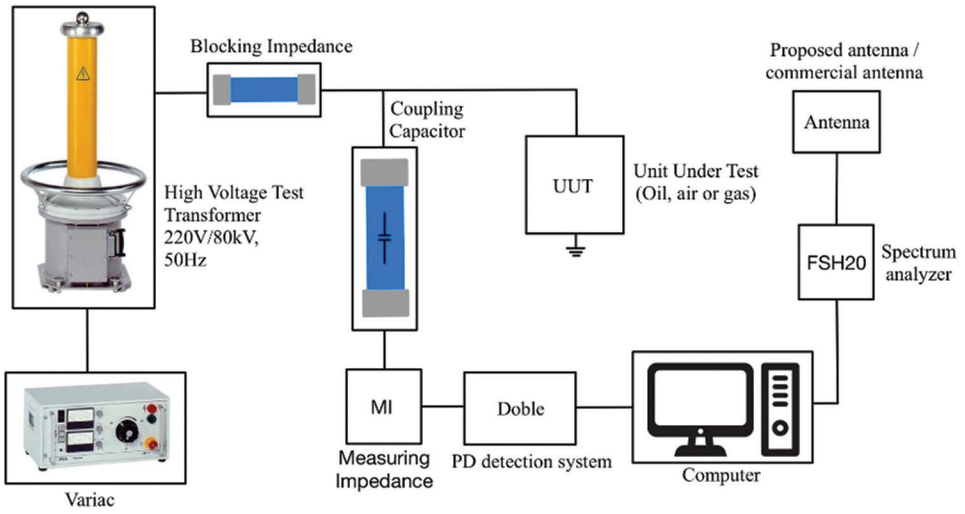

Fig. 9. Experimental setup to generate partial discharge signals.

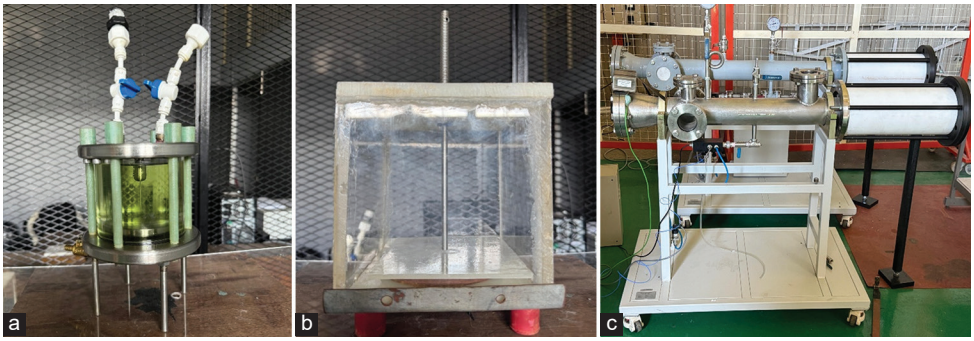

Fig. 10. Unit under test to generate partial discharge in (a) oil, (b) air, and (c) gas.

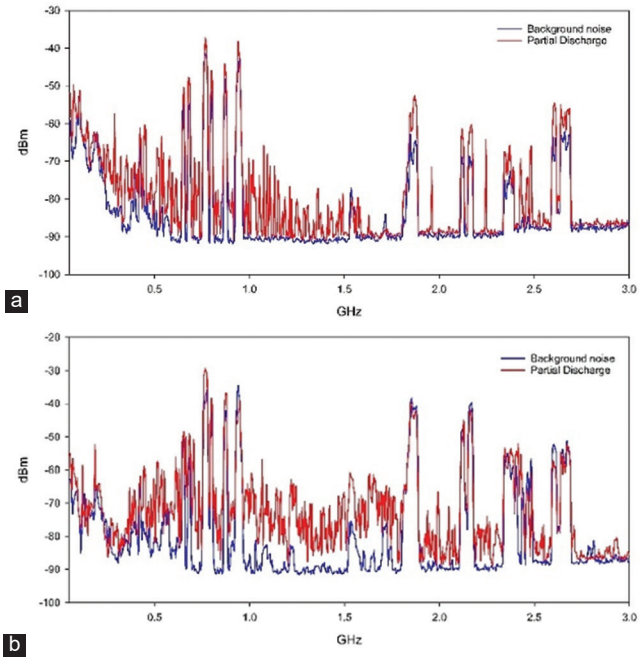

Fig. 11. Full span of partial discharge detection in oil for (a) Watson w-881 whip antenna and (b) proposed log-periodic dipole array antenna.

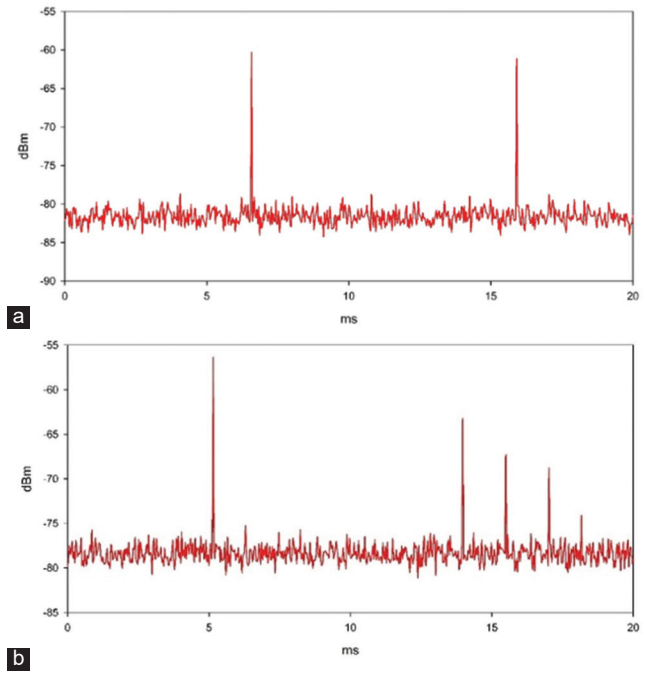

Fig. 12. Zero span of partial discharge detection in oil at 536 MHz using (a) Watson w-881 whip antenna and (b) proposed log-periodic dipole array antenna at 100 cm.

sharper responses, with peaks near −73 dBm, demonstrating improved sensitivity and clearer pulse definition at this lower frequency.

Fig. 19a and b present the PD detection results in an N_2O_2Ar gas environment using the commercial PDU-G2

http://dx.doi.org/10.14500/aro.12846

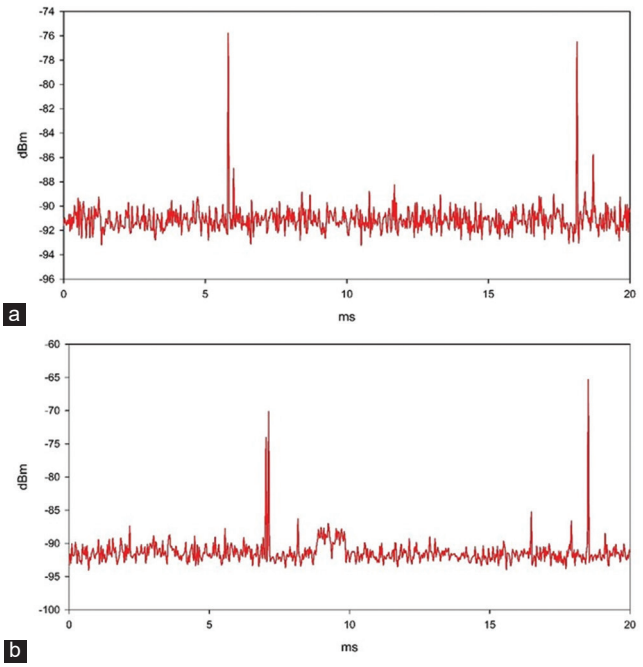

Fig. 13. Zero span of partial discharge detection in oil at 1 GHz using (a) Watson w-881 whip antenna and (b) proposed log-periodic dipole array antenna at 100 cm.

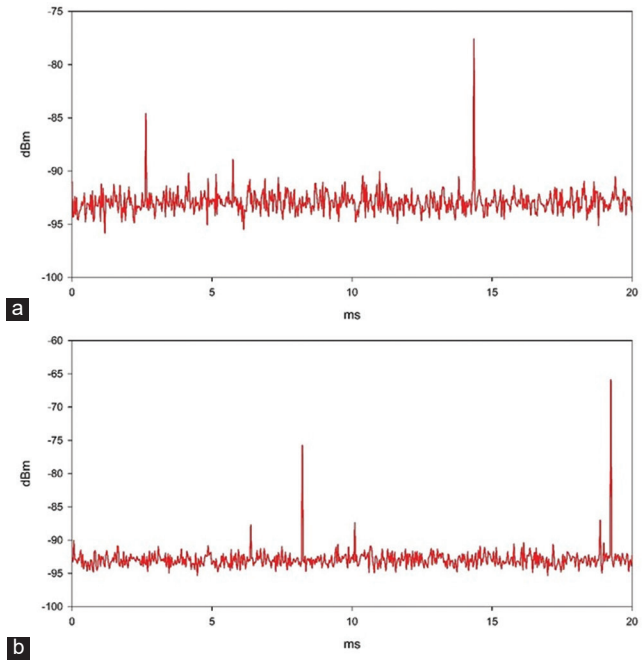

Fig. 14. Zero span of partial discharge detection in oil at 1.3 GHz using (a) Watson w-881 whip antenna and (b) proposed log-periodic dipole array antenna at 100 cm.

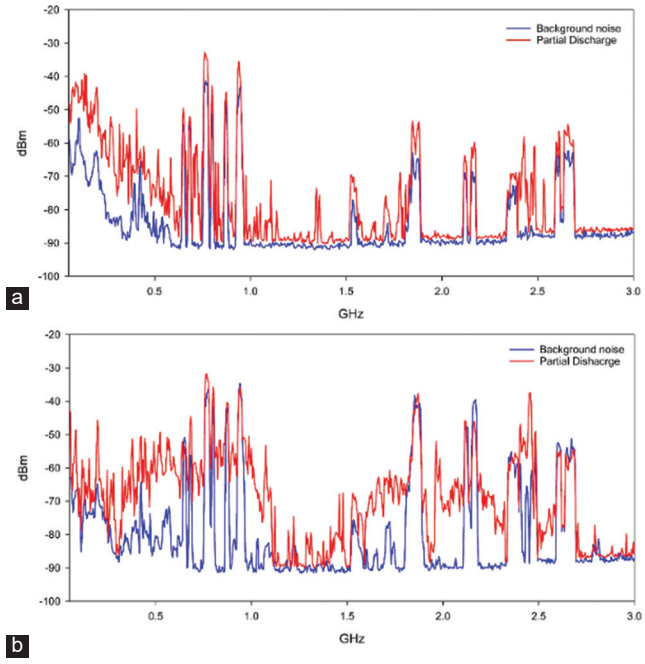

Fig. 15. Full span of partial discharge detection in air for (a) Watson w-881 whip antenna and (b) proposed log-periodic dipole array antenna.

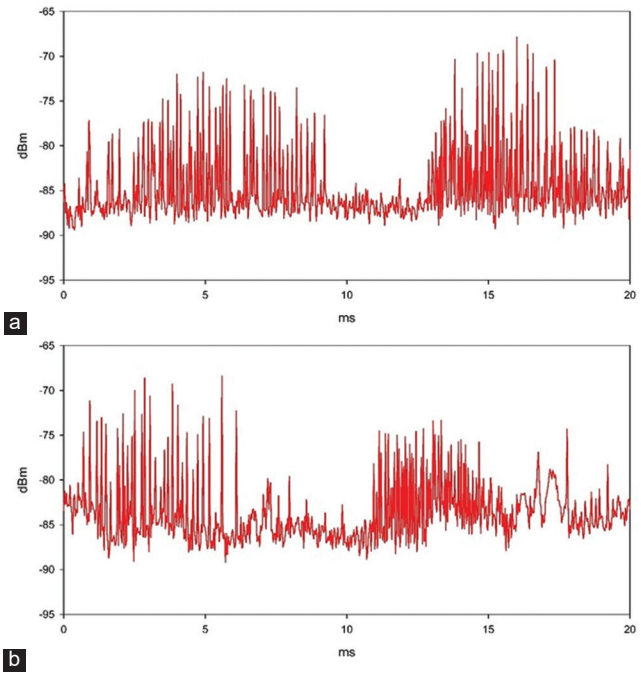

Fig. 16. Zero span of Partial discharge detection in air at 434 MHz using (a) Watson w-881 whip antenna and (b) proposed log-periodic dipole array antenna at 100 cm.

antenna and the proposed U-shaped patch LPDA antenna, respectively. For the PDU-G2, the background noise remained below −85 dBm with occasional interference, whereas PD activity produced clear spectral rises, particularly below 1 GHz, where peaks reached −65 dBm, and additional activity was observed up to 1.7 GHz. Similarly, the proposed antenna shows PD signals clearly distinguishable from the background across the lower and mid-frequency ranges, with noticeable separation between noise and discharge traces.

For the zero-span results in Fig. 20, the commercial antenna detects two dominant PD pulses with peaks around -80 dBm above a −93 dBm noise floor, indicating that only a few events rose clearly above the background. In comparison, the proposed antenna records multiple pulses with stronger signals of about −73–−75 dBm and a similar

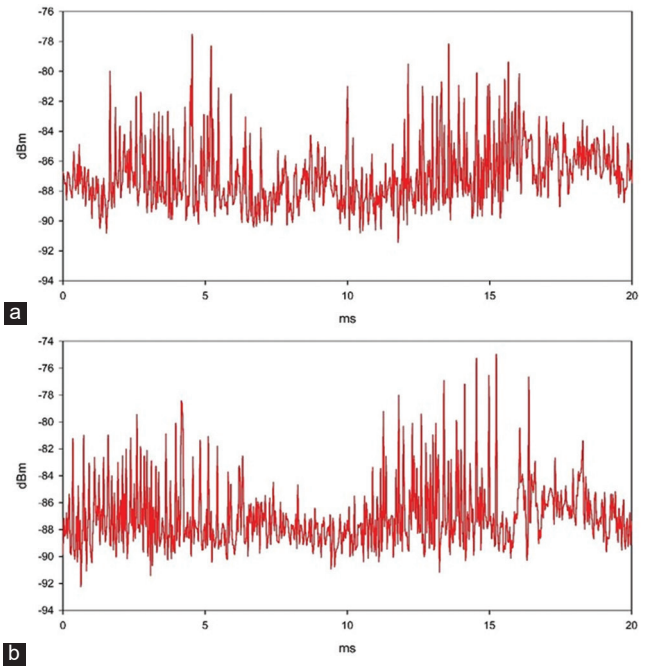

Fig. 17. Zero span of partial discharge detection in air at 499 MHz using (a) Watson w-881 whip antenna and (b) proposed log-periodic dipole array antenna at 100 cm.

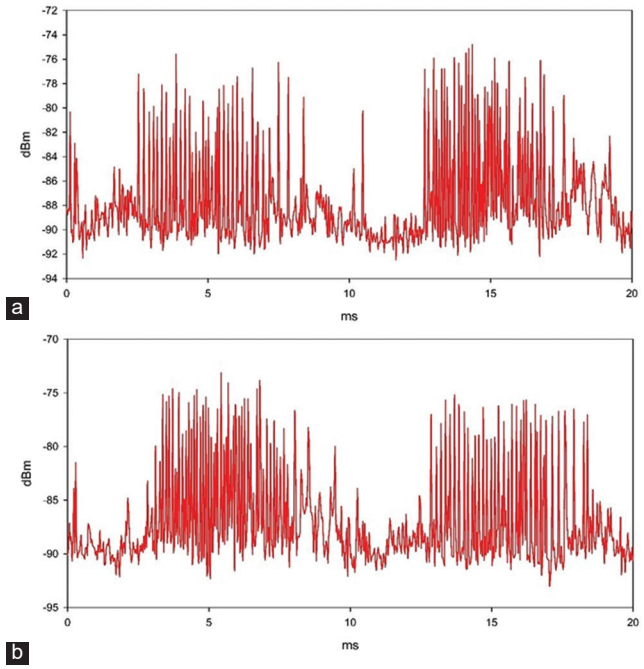

Fig. 18. Zero span of partial discharge detection in air at 510 MHz using (a) Watson w-881 whip antenna and (b) proposed log-periodic dipole array antenna at 100 cm.

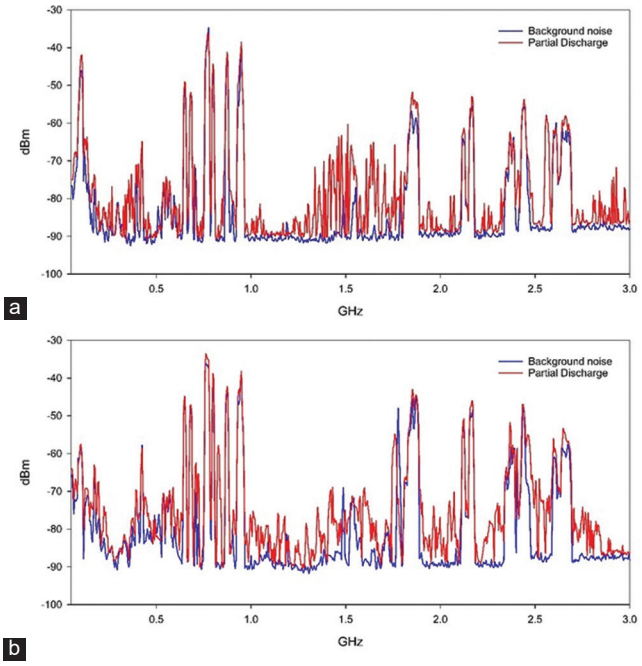

Fig. 19. Full span of partial discharge detection in N_2O_2Ar gas for (a) PDU-G2 external antenna and (b) proposed log-periodic dipole array antenna.

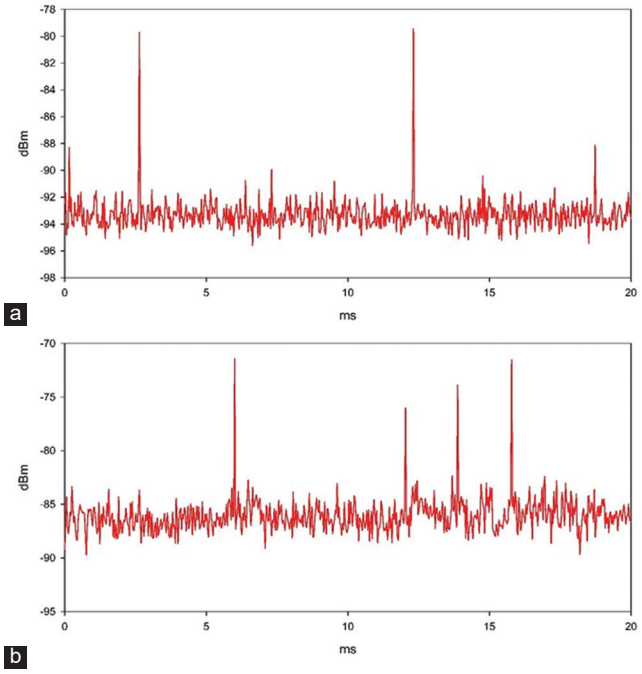

Fig. 20. Zero span of partial discharge detection in N_2O_2Ar gas at 440 MHz using (a) PDU-G2 external antenna and (b) proposed log-periodic dipole array antenna.

baseline. The increased number and strength of the pulses confirm the better sensitivity of the proposed antenna for detecting discharge activity in gas.

Based on Fig. 21, both antennas detected PD activity in the N_2O_2Ar gas mixture. The commercial antenna shows weak responses, with only a few peaks around −85–−86 dBm. In comparison, the proposed antenna records clearer and more frequent pulses with sharp peaks near −76 dBm, which demonstrates the higher sensitivity of the proposed antenna for PD detection in gas conditions.

Based on Fig. 22, both the commercial and proposed antennas detected PD pulses above the noise floor, but with clear differences in signal amplitude and consistency. The commercial antenna shows a few sharp peaks, with the

http://dx.doi.org/10.14500/aro.12846

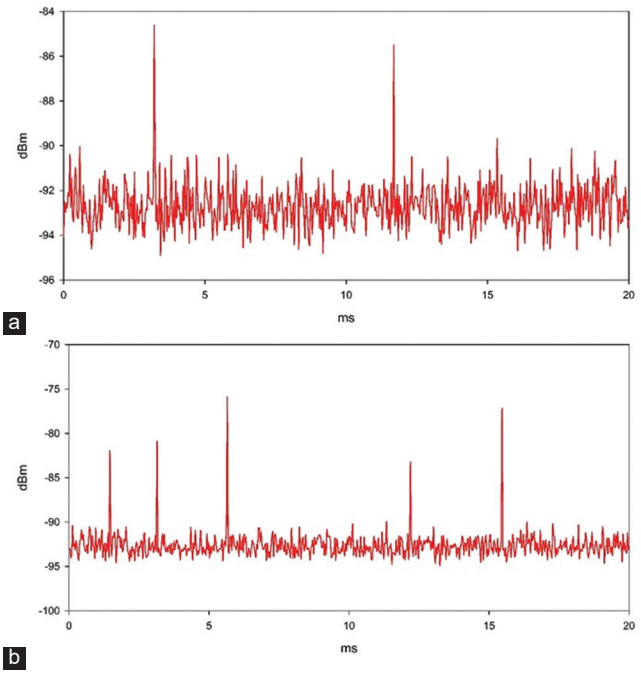

Fig. 21. Zero span of partial discharge detection in N_2O_2Ar gas at 1.01 GHz using (a) PDU-G2 external antenna and (b) proposed log-periodic dipole array antenna.

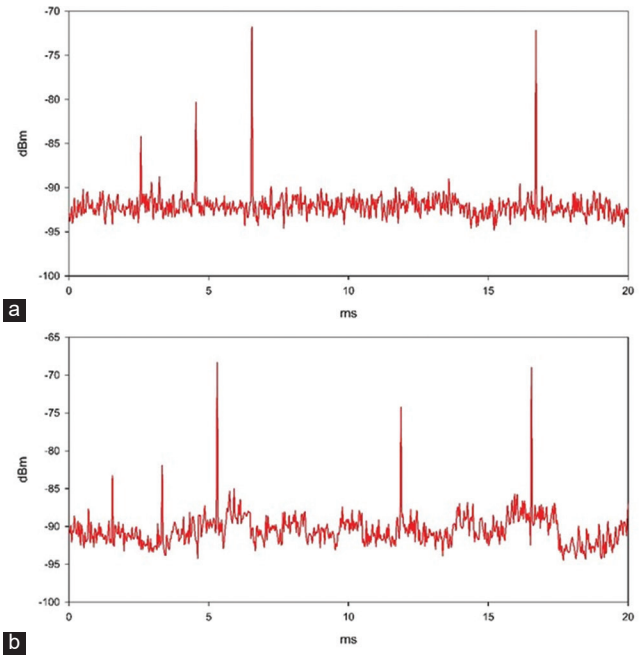

Fig. 22. Zero span of partial discharge detection in N_2O_2Ar gas at 1.42 GHz using (a) PDU-G2 external antenna and (b) proposed log-periodic dipole array antenna.

strongest near −72 dBm, whereas most pulses are weak and close to the noise level. In comparison, the proposed antenna records more pulses with higher amplitudes in the range of −68–−84 dBm and more regular repetition, which indicates a more reliable discharge detection.

B. Phase-resolved PD (PRPD) Pattern for Oil and Air Condition

The experiment is conducted to compare the PD signals detected by several sensors, including the conventional IEC 60270 measurement setup with a coupling capacitor and measuring impedance, an HFCT, a commercial whip antenna, and the proposed LPDA antenna, with the goal of cross-verification of PD signals under identical conditions. The HFCT is included to improve the reliability by allowing comparison with antenna-based measurements. The experimental setup is shown in Fig. 23.

As shown in Fig. 24, the PRPD patterns resulting from the coupling capacitor with measuring impedance, HFCT, and the proposed LPDA antenna are similar, with pulses near 90° and 270°, which indicates corona discharge. While the coupling capacitor and HFCT measure current-related signals, the proposed LPDA antenna reproduces the same phase pattern using radiated signal measurements. Despite differences in amplitude scale, the comparable patterns demonstrate that the proposed antenna can reliably capture corona activity consistent with conventional methods.

Fig. 25 demonstrates the PRPD patterns resulting from coupling a capacitor with measuring impedance, HFCT, and the proposed LPDA antenna in the air condition. The PRPD results for the air condition indicate that all three sensors detected activity primarily in the first and third quadrants of the voltage cycle. The coupling capacitor recorded strong discharges with higher density in the positive half cycle, whereas the HFCT detected the same phase positions with lower charge magnitudes. The proposed LPDA antenna reproduced the same distribution, with pulses in both half cycles and greater density during the positive cycle. Although expressed in millivolts rather than charge, the results are consistent with the conventional methods, confirming that the proposed antenna can reliably detect surface discharge.

In addition, practical factors such as insulation safety, electromagnetic interference, and installation position should be considered since the antenna is designed for HV monitoring. The antenna can be installed outside the HV area when detecting PD, which reduces the risk from direct electrical contact. Furthermore, proper installation and shielding may further enhance the measurement reliability.

Although the proposed antenna shows strong broadband performance and size reduction, some practical limitations exist. The use of lumped inductors introduces parasitic effects and component tolerances that may slightly affect performance at higher frequencies. In extreme environments with high interference or harsh conditions, additional shielding or calibration may be required. Future work will investigate long-term stability and robustness in real industrial settings.

V. Performance Comparison

As presented in Table 2, the key parameters, including antenna dimensions, frequency range, gain, S_{11}, and fractional bandwidth (FBW), are compared between the proposed

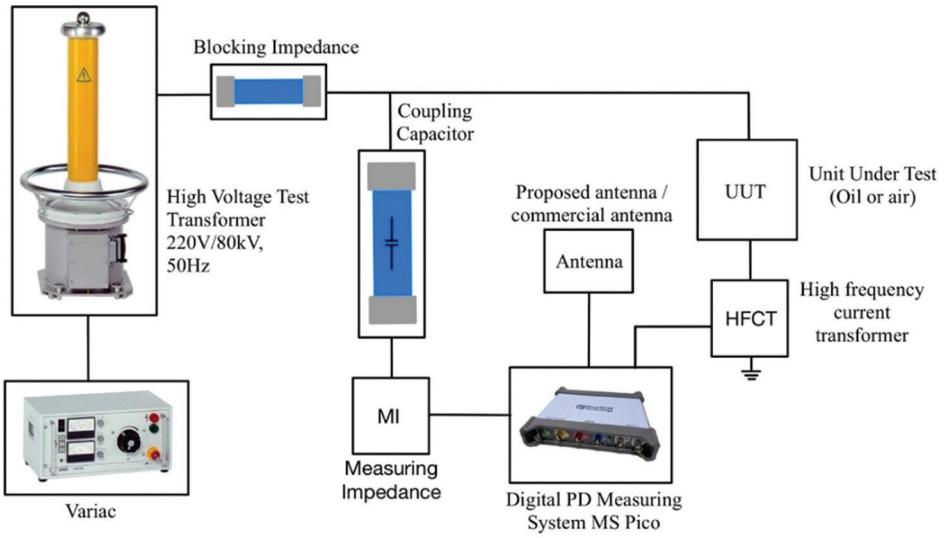

Fig. 23. The experimental setup to validate the partial discharge signal detected by various sensors.

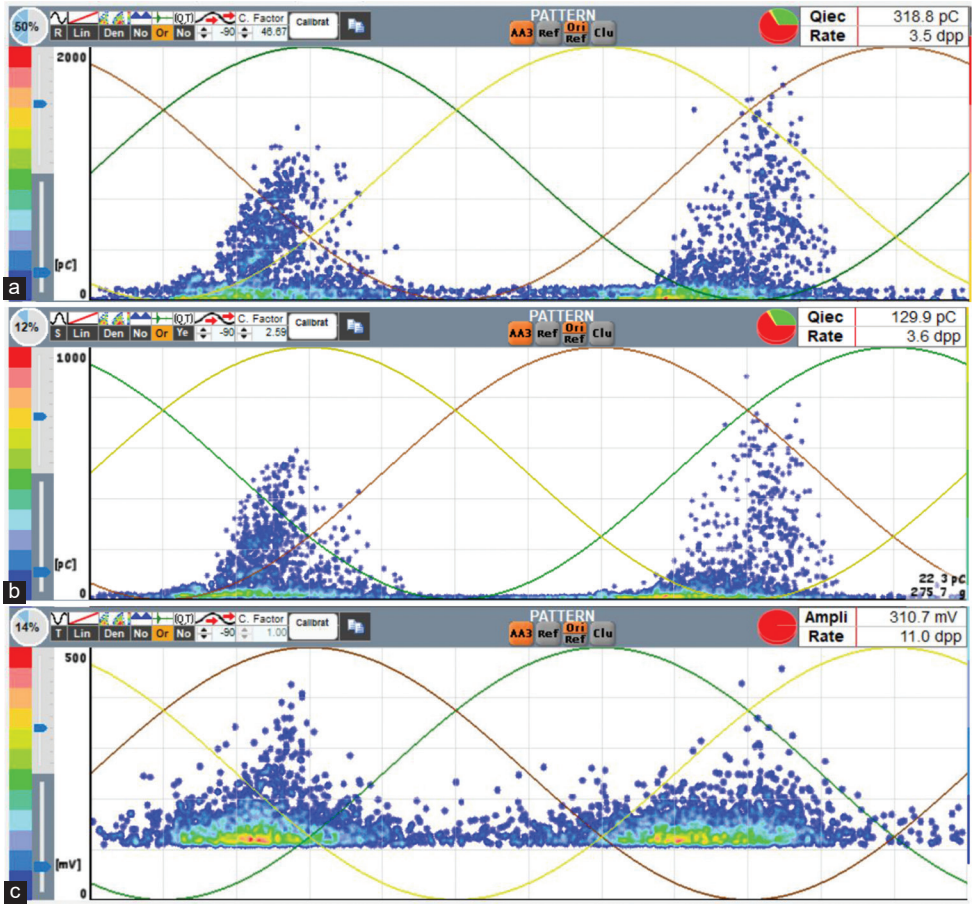

Fig. 24. Phase-resolved partial discharge patterns under the same test conditions in oil using (a) coupling capacitor with measuring impedance, (b) high-frequency current transformer, and (c) U-shaped patch log-periodic dipole array antenna.

antenna and other antennas reported in previous studies. The proposed LPDA antenna operates from 0.44 GHz to 2.75 GHz with a peak gain of 5.6 dBi and an FBW of 145%, which outperforms those previously reported designs. While some earlier antennas exhibit multiple bands with lower gains and smaller bandwidths, the proposed design offers a compact size of 300 × 200 mm (1.60 λ × 1.06 λ) and improved overall performance in terms of bandwidth and peak gain, demonstrating its effectiveness for wideband applications.

On the other hand, the proposed antenna structure can also be extended to higher frequency applications by appropriately scaling the LPDA geometrical parameters and modifying the

 http://dx.doi.org/10.14500/aro.12846

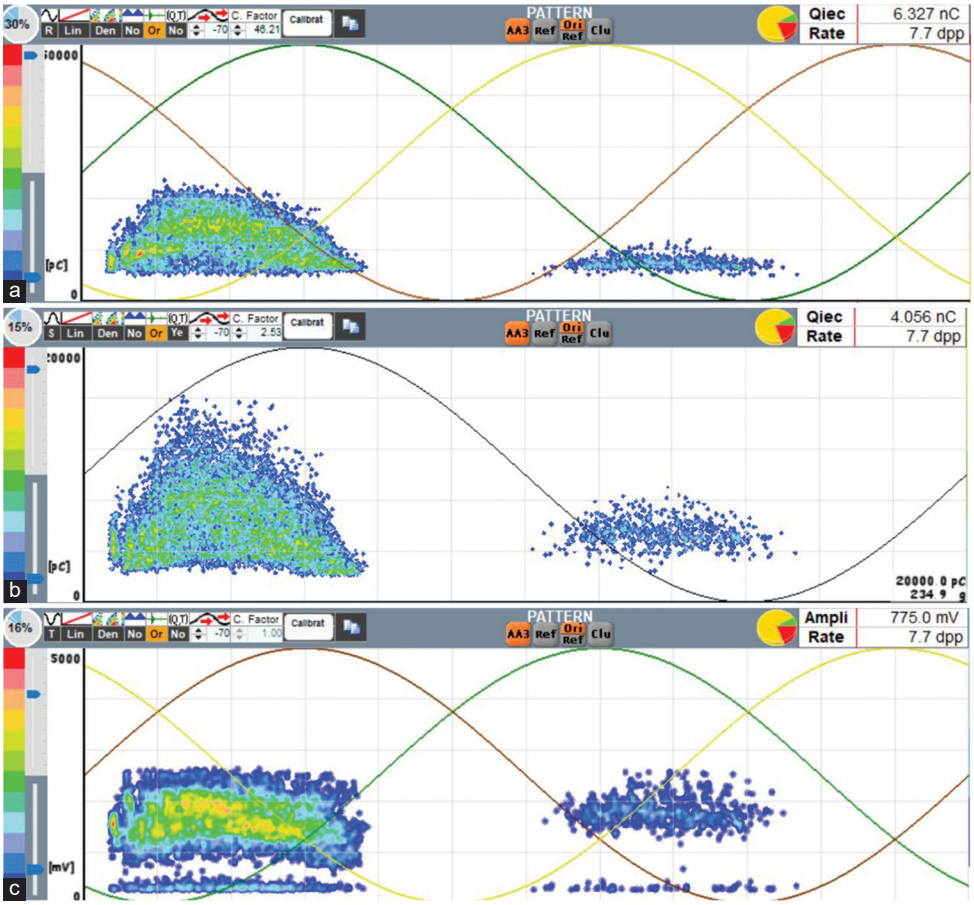

Fig. 25. Phase-resolved partial discharge patterns under the same test conditions in air using (a) coupling capacitor with measuring impedance, (b) high-frequency current transformer, and (c) proposed log-periodic dipole array antenna.

TABLE II
PERFORMANCE COMPARISON OF THE DESIGNED ANTENNA WITH PREVIOUS REPORTED ANTENNAS IN THE LITERATURE

References	Antenna size (Area)	Dimension (mm²)	Frequency range (GHz)	Gain (dBi)	S_{11} (dB)	FBW (%)
(Kong, et al., 2024)	0.54 λ_o×0.51 λ_o	200×187	0.5–1.12	4.6 (peak)	−10	76.5
(Ahmed, et al., 2024)	0.67 λ_o×0.58 λ_o	240×210	0.37–1.30	3.96 (peak)	−10	111
(Ardila-Rey, et al., 2024)	0.99 λ_o×0.52 λ_o	274×144	0.45–1.71	1.36–4.45	−10	116.7
(Uwiringiyimana, Khayam, and Montanari, 2024)	0.54 λ_o×0.47 λ_o	80×70	1.44–2.59	-	−10	57
(Yadam, Sarathi, and Arunachalam, 2022)	0.26 λ_o	154	1.44–2.59	1–4.95	−10	163.6
(Salah, et al., 2022)	2.57 λ_o×2.57 λ_o, 5.11 λ_o×5.11 λ_o, 7.76 λ_o×7.76 λ_o, 10.65 λ_o×10.65 λ_o	90×90	0.67–1.04, 1.4–2.0, 2.3–2.89, 3.1–4.0	-	−10	44, 35, 22.5, 25.4
(Chakravarthi, et al., 2021)	0.50 λ_o×0.63 λ_o	110×140	0.5–2.2	4	−10	126
This work	1.60 λ_o×1.06 λ_o	300×200	0.44–2.75	5.6 (peak)	−10	145

FBW: Fractional bandwidth, S_{11}: Reflection coefficient

lumped element values. Since the LPDA design is governed by scaling factors, operation at higher frequencies mainly requires proportional reduction of the element dimensions. However, at elevated frequencies, the influence of lumped component parasitics and fabrication tolerances becomes more significant and should be considered in future optimization.

VI. CONCLUSION

This work successfully demonstrated the miniaturized U-shaped LPDA antenna integrated with lumped inductors for PD detection in oil, air, and gas environments. The antenna achieved a significant size reduction of 63.3%, with a final dimension of 300 × 220 mm² compared to conventional LPDA structures. The measured reflection coefficient highlighted that the proposed antenna can operate from 0.44 GHz to 2.75 GHz, covering the UHF PD detection spectrum defined in IEC 62478. Furthermore, this design exhibited a measured gain between 4 dBi and 5.6 dBi, demonstrating a stable radiation performance across the operating band.

Experimental validation confirmed that the proposed antenna can capture PD signals with comparable or improved sensitivity

relative to a commercial antenna. Zero span spectrum analysis and PRPD pattern comparisons showed clear PD detection with improved noise immunity and broadband coverage. In conclusion, the proposed antenna offers enhanced bandwidth, size reduction, and multi-detection capability, making the proposed antenna suitable for HV monitoring sensors.

VII. Acknowledgment

This work was supported in part by the Higher Institution Centre of Excellence (HICOE), Ministry of Higher Education Malaysia, through the Wireless Communication Centre (WCC), Universiti Teknologi Malaysia (UTM), under Grant R.J130000.7823.4J610; and in part by the UTM Fundamental Research (UTMFR) under Grant Q.J130000.3823.23H92; and in part by the EU HORIZON MSCA-SE project TRACE-V2X under Grant Agreement No. 101131204.

References

Ahmed, N., and Srinivas, N., 2002. On-line partial discharge detection in cables. *IEEE Transactions on Dielectrics and Electrical Insulation*, 5, pp.181-188.

Ahmed, R., Abd-Rahman, R., Ullah, Z., Ullah, R., Yousof, M.F., and Ullah, K., 2024. Partial discharge characterization of HFO(E) gas using ultra-high frequency (UHF) antenna for medium voltage switchgear application. *IEEE Access*, 12, pp.81196-81205.

Ardila-Rey, J.A., Figueroa, D., Torres, F.P., Govindarajan, S., De Castro, B.A., and Schurch, R., 2024. Bioinspired ultra high frequency antenna for partial discharge detection in high-voltage equipment. *IEEE Transactions on Instrumentation and Measurement*, 73, pp.1-18.

Ashari, F., and Khayam, U., 2017. *2017 4th International Conference on Electric Vehicular Technology (ICEVT)*. IEEE.

Balanis, C.A., 2016 *Antenna Theory: Analysis and Design*. John Wiley and Sons, New Jersey.

Biswas, S., Koley, C., Chatterjee, B., and Chakravorti, S., 2012. A methodology for identification and localization of partial discharge sources using optical sensors. *IEEE Transactions on Dielectrics and Electrical Insulation*, 19, pp.18-28.

Chakravarthi, M.K., Giridhar, A., Kumar, G.A., and Sarma, D.S., 2021. A compact log periodic planar dipole UHF array sensor for partial discharge measurements. *IEEE Sensors Journal*, 21(24), pp.27748-27756.

Chishti, A.R., Aziz, A., Aljaloud, K., Tahir, F.A., Abbasi, Q.H., Khan, Z.U., and Hussain, R., 2023. A sub 1 GHz ultra miniaturized folded dipole patch antenna for biomedical applications. *Scientific Reports*, 13(1), p.9900.

Descoeudres, A., Hollenstein, C., Demellayer, R., and Wälder, G., 2004. Optical emission spectroscopy of electrical discharge machining plasma. *Journal of Physics D: Applied Physics*, 37(6), p.875.

Duval, M., 2002. A review of faults detectable by gas-in-oil analysis in transformers. *IEEE Electrical Insulation Magazine*, 18(3), pp.8-17.

Hampton, B., and Meats, R., 1988. *IEE Proceedings C (Generation, Transmission and Distribution)*. IET.

Hoshino, T., Koyama, H., Maruyama, S., and Hanai, M., 2006. Comparison of sensitivity between UHF method and IEC 60270 for onsite calibration in various GIS', *IEEE Transactions on Power Delivery*, 21(4), pp.1948-1953.

Hu, X., Zhang, G., Liu, X., Chen, K., and Zhang, X., 2023. Design of high-sensitivity flexible low-profile spiral antenna sensor for GIS built-in PD detection. *Sensors*, 23(10), p.4722.

Ilkhechi, H.D., and Samimi, M.H., 2021. Applications of the acoustic method in partial discharge measurement: A review. *IEEE Transactions on Dielectrics and Electrical Insulation*, 28(1), pp.42-51.

Kong, X., Zhang, C., Hou, C., Lin, X., and Du, B., 2024. UHF sensor for partial discharge detection based on coplanar waveguide feeding. *IEEE Sensors Journal*, 24, pp.28119-28128.

Kusumoto, S., Itoh, S., Tsuchiya, Y., Mukae, H., Matsuda, S., and Takahashi, K., 1980. Diagnostic technique of gas insulated substation by partial discharge detection. *IEEE Transactions on Power Apparatus and Systems*, 99(4), pp.1456-1465.

Luo, Q., Pereira, J.R., and Salgado, H., 2011. Compact printed monopole antenna with chip inductor for WLAN. *IEEE Antennas and Wireless Propagation Letters*, 10, pp.880-883.

Mishra, D., Sarkar, B., Koley, C., and Roy, N., 2015. *2015 Annual IEEE India Conference (INDICON)*. IEEE.

Muru, A., and Setijadi, E., 2023. *2023 International Seminar on Intelligent Technology and Its Applications (ISITIA)*. IEEE.

Riera-Guasp, M., Antonino-Daviu, J.A., and Capolino, G.A., 2014. Advances in electrical machine, power electronic, and drive condition monitoring and fault detection: State of the art. *IEEE Transactions on Industrial Electronics*, 62(3), pp.1746-1759.

Rutgers, W., and Fu, Y., 1997. *UHF PD-Detection in a Power Transformer*. U.S. Department of Energy, Washington, DC.

Salah, W.S., Gad, A.H., Attia, M.A., Eldebeikey, S.M., and Salama, A.R., 2022. Design of a compact ultra-high frequency antenna for partial discharge detection in oil immersed power transformers. *Ain Shams Engineering Journal*, 13(2), p.101568.

Schwarz, R., Muhr, M., and Pack, S., 2005. *IEEE International Conference on Dielectric Liquids, 2005. ICDL 2005.* IEEE.

Standard, I., 2000. *High-Voltage Test Techniques: Partial Discharge Measurements. IEC-60270*. IEC, Geneva, pp.13-31.

Stone, G.C., 2012. A perspective on online partial discharge monitoring for assessment of the condition of rotating machine stator winding insulation. *IEEE Electrical Insulation Magazine*, 28(5), pp.8-13.

Su, S.W., 2018. Capacitor-inductor-loaded, small-sized loop antenna for WLAN notebook computers. *Progress In Electromagnetics Research M*, 71, pp.179-188.

Tenbohlen, S., Denissov, D., Hoek, S.M., and Markalous, S., 2008. Partial discharge measurement in the ultra high frequency (UHF) range. *IEEE Transactions on Dielectrics and Electrical Insulation*, 15(6), pp.1544-1552.

Tenbohlen, S., Gulski, E., and Koltunowicz, W., 2016. *Guidelines for Partial Discharge Detection using Conventional (IEC60270) and Unconventional Methods*. Electra, pp.25-29.

Uwiringiyimana, J.P., Khayam, U., and Montanari, G.C., 2024. Planar rectangular microstrip antenna for partial discharge detection: Experimental validation on oil-filled transformer tank. *IEEE Access*, 12, pp.133199-133208.

Wang, F., Bin, F., Sun, Q., Fan, J., Liang, F., and Xiao, X., 2017. A novel uhf m inkowski fractal antenna for partial discharge detection. *Microwave and Optical Technology Letters*, 59(8), pp.1812-1819.

Wang, P., Ma, S., Akram, S., Zhou, K., Chen, Y., and Nazir, M.T., 2020. Design of archimedes spiral antenna to optimize for partial discharge detection of inverter fed motor insulation. *IEEE Access*, 8, pp.193202-193213.

Wang, Y., Wang, Z., and Li, J., 2016. UHF Moore fractal antennas for online GIS PD detection. *IEEE Antennas and Wireless Propagation Letters*, 16, pp.852-855.

Wu, M., Cao, H., Cao, J., Nguyen, H.L., Gomes, J.B., and Krishnaswamy, S.P., 2015. An overview of state-of-the-art partial discharge analysis techniques for condition monitoring. *IEEE Electrical Insulation Magazine*, 31(6), pp.22-35.

Xia, Y., Li, Y., and Xue, W., 2020. A low profile miniaturization low frequency wideband antenna using passive lumped elements loading. *Applied Computational Electromagnetics Society Journal*, 35, pp.31-37.

Yadam, Y.R., Sarathi, R., and Arunachalam, K., 2022. Planar ultrawideband circularly polarized cosine slot Archimedean spiral antenna for partial discharge detection. *IEEE Access*, 10, pp.35701-35711.